


Antisite disorder in the battery material LiFePO₄J. Werner¹, C. Neef¹, C. Koo¹, S. Zvyagin², A. Ponomaryov² and R. Klingeler^{1,3,*}¹Kirchhoff Institute of Physics, Heidelberg University, INF 227, D-69120 Heidelberg, Germany²Dresden High Magnetic Field Laboratory (HLD-EMFL), Helmholtz-Zentrum Dresden Rossendorf, D-01328 Dresden, Germany³Centre for Advanced Materials (CAM), Heidelberg University, INF 225, D-69120 Heidelberg, Germany (Received 15 April 2020; revised 9 June 2020; accepted 11 August 2020; published 25 November 2020)

We report detailed magnetometry and high-frequency electron spin resonance (HF-ESR) measurements which allow detailed investigation on Li-Fe antisite disorder in single-crystalline LiFePO₄, i.e., exchange of Fe²⁺ and Li⁺ ions. The data imply that magnetic moments of Fe²⁺ ions at Li positions do not participate in long-range antiferromagnetic order in LiFePO₄ but form quasifree moments. Anisotropy axes of the magnetic moments at antisite defects are attached to the main crystallographic directions. The local character of these moments is confirmed by associated linear resonance branches detected by HF-ESR studies. Magnetic anisotropy shows up in significant zero-field splittings of $\Delta = 220(3)$ GHz, $\Delta' \sim 50$ GHz, and a highly anisotropic g factor, i.e., $g_a = 1.4$, $g_b = 2.0$, and $g_c = 6.3$. We demonstrate a general method to precisely determine Fe-antisite disorder in LiFePO₄ from magnetic studies which implies a density of paramagnetic Fe²⁺ ions at Li positions of 0.53%.

DOI: [10.1103/PhysRevMaterials.4.115403](https://doi.org/10.1103/PhysRevMaterials.4.115403)

I. INTRODUCTION

Electronic and ionic conductivity crucially affect the performance of electrode materials for lithium-ion batteries (LIB), including the charge and discharge rates, cycling stability, and practically accessible capacity. Therefore, it is essential to understand the properties of defects unavoidably appearing in real materials as a precondition to understanding conductivity and eventually battery performance. In systems like the commercialised battery material LiFePO₄, where ionic diffusion is supposed to be promoted along channels of the lattice structure, i.e., of one-dimensional (1D) nature, defects particularly affect actual conductivity as channels are easily blocked [1]. However, defects are not necessarily detrimental to high-performance electrodes but may significantly enhance it by enabling additional low-energy ionic pathways [2,3]. This is particularly true for Li-Fe antisite disorder which is an intrinsic type of defect in olivinelike transition metal phosphates. Due to the similar covalent radii of Li and Fe ions, both can change places and form a so-called antisite defect. Calculations in Ref. [4] suggest that ionic migration perpendicular to the 1D channels is energetically more favorable than along the blocked channels, and might even yield ionic migration of higher dimensionality by supporting channel crossover [1,3]. In this respect, activation energies for ionic diffusion along the crystallographic directions perpendicular to the channels can be interpreted as activation of channel crossover via antisite defects [5]. It has been shown that the essentially 1D transport in LiFePO₄ becomes three dimensional (3D) when the percolation threshold of only a few percent of antisite disordered Li/Fe positions is reached [6] which evidently would have strong implication for

understanding and designing actual battery materials. Ionic migration of higher dimensionality is indeed observed experimentally in single crystals studies [7,8]. Understanding the nature of Li-Fe antisite defects is hence crucial to calculate relevant input parameters for modeling LiFePO₄ as an electrode material [9].

Experimental studies on antisite disorder are challenging as conventional x-ray scattering is not sensitive to Li. In this paper we apply magnetic probes to study the intrinsic properties of antisite defects in LiFePO₄ single crystals, i.e., tunable high magnetic field/high-frequency electron spin resonance (HF-ESR) spectroscopy and static magnetization. We exploit the fact that antisite defects are magnetic in a sense that paramagnetic Fe ions reside in different crystallographic environments (Fig. 1) and are hence distinguishable and detectable while, at low-temperatures below the magnetic ordering temperature, Li ions form local nonmagnetic defects in the long-range antiferromagnetic ordered magnetic lattice of Fe moments. We show that the density of antisite defects is straightforwardly and precisely determined. In addition, energy levels of the Fe²⁺ ions at the Li position are studied in high magnetic fields by HF-ESR. We observe significant zero-field splittings of $\Delta' \sim 50$ GHz and $\Delta = 220(3)$ GHz of antisite Fe²⁺ moments and highly anisotropic effective g values along the different crystallographic axes, i.e., $g_a = 1.4$, $g_b = 2.0$, and $g_c = 6.3$ for the a , b , and c axis, respectively (space group $Pnma$). This anisotropy of the g factor is resembled by magnetic susceptibility which shows a strongly anisotropic Curie-Weiss-like upturn at low temperatures.

II. EXPERIMENT

Single crystals of LiFePO₄ were grown by the high-pressure optical floating-zone method as reported in detail in Ref. [10]. Magnetization in static magnetic fields up to 7 T

*r.klingeler@kip.uni-heidelberg.de

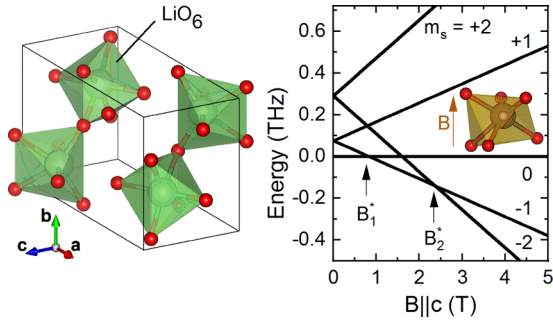


FIG. 1. (a) The four different LiO_6 octahedra of the LiFePO_4 unit cell. (b) Simplified energy-level diagram and crystal environment of the Fe-antisite defects with magnetic field applied along the crystallographic c direction. Crystal structure visualizations were generated with VESTA [12].

was studied by means of a Quantum Design MPMS-3 SQUID magnetometer. HF-ESR measurements were performed in a transmission type ESR spectrometer in Faraday geometry. ESR measurements in static fields up to 16 T were done by means of a phase-sensitive millimeter-wave vector network analyzer (MVNA) from AB Millimet re [11]. HF-ESR experiments in pulsed fields up to 50 T were performed at the Dresden High Magnetic Field Laboratory (HLD) using VDI modular transmitters (product of Virginia Diodes Inc., USA) as sub-mm radiation sources and InSb hot-electron bolometer as a radiation detector.

III. RESULTS

A. Magnetization

LiFePO_4 exhibits long range antiferromagnetic order of the $S = 2$ spins of the magnetic Fe^{2+} ions, which evolves at $T_N = 50.0(5)$ K [13–16]. In the ordered phase, the spins are mainly directed along the crystallographic b axis [17] with a small collinear rotation towards the a axis and spin canting along the c axis with an overall rotation of the ordered moments of $1.3(1)^\circ$ off the b axis [18,19]. The onset of magnetic order, i.e., T_N , is reflected by kinks in the static magnetic susceptibility $\chi = M/B$ shown in Fig. 2, and the easy axis $B||b$ is evident from Fig. 2(b) from the pronounced decrease in susceptibility upon cooling to 2 K. Notably, in contrast to rather constant values of χ , which are expected for a typical antiferromagnet [20], the susceptibility $\chi(B = 0.1 \text{ T}||c)$, i.e., applied along the hard axis, strongly increases upon cooling [see Fig. 2(a)]. We note that this magnetic field is far below any metamagnetic transition in LiFePO_4 [14]. In contrast, there is only a weak temperature dependence for $B||a$ axis (intermediate axis). Phenomenologically, the strong upturn of χ_c is described by a Curie-Weiss law $\chi_c = C_c/(T + \Theta_c)$, with the Curie constant $C_c = 0.179(3)$ erg K $\text{G}^{-2} \text{mol}^{-1}$ and the Weiss-temperature $\Theta_c = 6.5(1)$ K [see black line in Fig. 2(a)]. A constant background of $\chi_0 = 1.28610 \cdot 10^{-2}$ erg/ $\text{G}^2 \text{mol}$ was assumed to describe the susceptibility of the main system up to 20 K as suggested by the constant order parameter in this temperature range [18]. The Curie-Weiss law suggests the presence of only weakly correlated (i.e., “quasifree” with respect to the main antiferromagnetic ordering phenomenon at

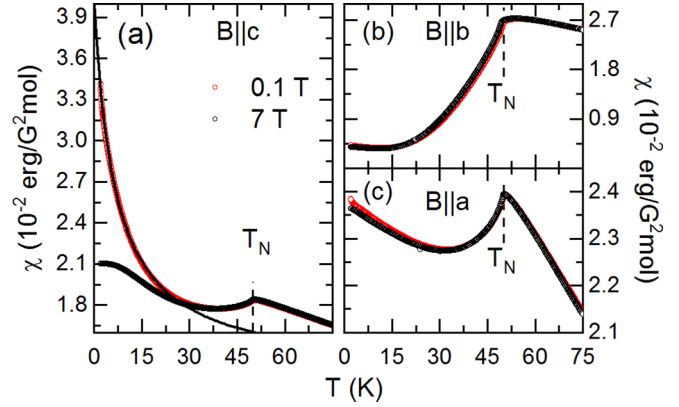


FIG. 2. Static magnetic susceptibility at $B = 0.1$ and 7 T with external magnetic fields applied along (a) $B||c$, (b) $B||b$, and (c) $B||a$. The dashed lines indicate the N el-temperature $T_N = 50$ K of LiFePO_4 at 0.1 T. The solid black line in (a) is a Curie-Weiss fit of the data (see the text).

T_N) magnetic moments which do not participate in long-range antiferromagnetic spin order. The fact that only a weak Curie-like increase is observed below 30 K for the other directions implies the anisotropic nature of these quasifree spins [21]. This is confirmed by application of $B = 7$ T which nearly does not affect χ_a and χ_b while the steep upturn in χ_c is suppressed towards a rather expected behavior. T_N is almost unchanged either. Please note that interpreting the steep upturn as the response of moments not involved in the overall spin structure implies that the parameters obtained by Curie-Weiss fitting must be taken cautiously as the response of the long-range order phase is not precisely known. As will be shown, precise quantitative separation is feasible if $M(B)$ data are exploited.

Anisotropy of the low-temperature magnetization is further elucidated in Fig. 3, where the susceptibility at $T = 2$ K is shown in dependence of the field direction for $B = 0.1$ and 7 T. At $B = 7$ T, the expected behavior for antiferromagnets is observed, i.e., the susceptibility is smallest for $B||b$ (easy

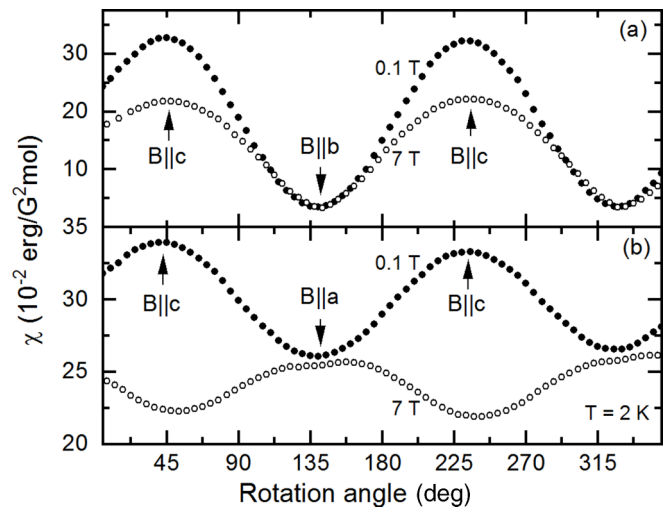


FIG. 3. Static magnetic susceptibility at $B = 0.1$ and 7 T, at $T = 2$ K, with external magnetic fields applied (a) in the bc plane and (b) in the ac plane. Arrows indicate the main crystallographic directions.

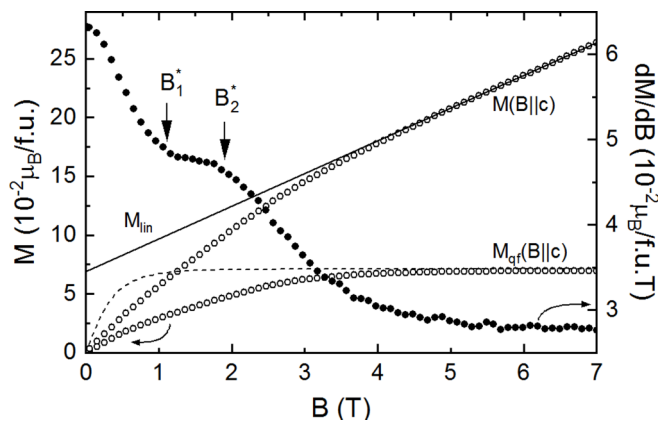


FIG. 4. Magnetization (left axis) and its derivative $\partial M/\partial B$ (right axis), at $T = 1.8$ K, for $B||c$. $M_{\text{qf}} = M - M_{\text{lin}}$ is the difference between the measured magnetization M and high-field linear contribution M_{lin} (see solid line), the dashed line represent a fit to M_{qf} by means of the Brillouin function and B_1^* , B_2^* mark anomalies in $\partial M/\partial B$.

axis) while it is highest for $B||a$ (intermediate axis). This differs from the finding at small magnetic field where the quasifree moments significantly contribute. At $B = 0.1$ T, the susceptibility is almost unchanged with respect to the high-field values for $B||b$ and $B||a$. In contrast, χ_c is much larger which must be attributed to the quasifree moments. The data hence imply that the g tensor of the quasifree moments is strongly anisotropic and attached to the main crystallographic directions of LiFePO_4 . The discrepancies of minima and maxima for the different measurements are within the error bars of the MPMS-3 rotor of approximately 5° .

Measurements of the magnetization in dependence of the external magnetic field (Fig. 4) reflect the unusual anisotropic behavior of the low-temperature susceptibility as well. While for magnetic fields $B \perp c$ only tiny right bending is observed, significant curvature is only observed for $B||c$ (cf. Ref. [14]). This right bending is superimposed by a linear-in-field contribution to the magnetization up to the highest measured fields of ≥ 56 T [14], except for metamagnetic transitions appearing at $B||b \sim 32$ T. Such linear field effect is typical for three-dimensional antiferromagnets and is attributed to the response of the antiferromagnetically ordered spins $S = 2$. In contrast, right bending at rather low energy fields clearly signals the alignment of magnetic moments which are not expected in a conventional antiferromagnet. Note that these extra moments are not explained by small canting of the Fe spins of $\alpha = 1.3^\circ$ away from the easy b axis [18,19] as will be shown below by HF-ESR data.

In order to further analyze the observed quasifree moments, we have separated the nonlinear from the linear part by fitting the high-field behavior with a linear function and subtracted the resulting straight line from the data [22]. This procedure gives $M_{\text{qf}} = M - M_{\text{lin}}$ as shown in Fig. 4. It shows the alignment of quasifree moments towards their saturation value of $M_{\text{qf}}^{\text{sat}} = 0.071(1) \mu_B/\text{f.u.}$ at around 5.5 T. This is in-line with the χ vs T data in Fig. 2(a) which imply suppression of the steep Curie-like upturn at 7 T. The data presented in Figs. 2 and 4 hence clearly evidence the presence of only

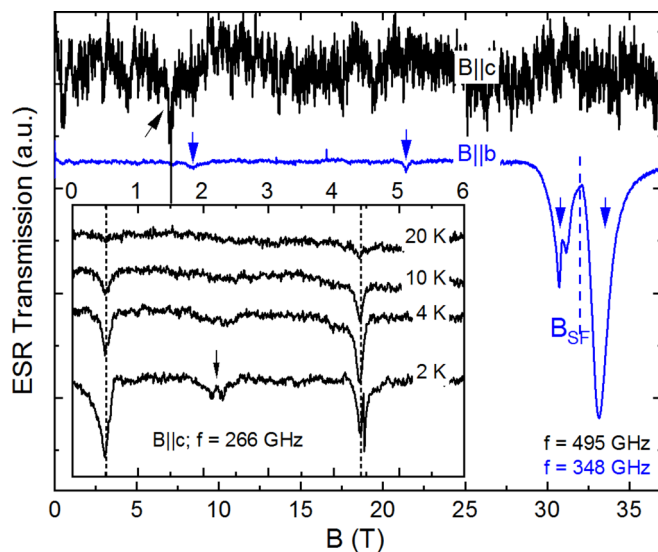


FIG. 5. High-frequency electron spin resonance spectra in pulsed fields $B||c$ and $B||b$ at $f = 495$ GHz and $f = 348$ GHz, respectively, measured at $T \sim 4$ K. The dashed line indicates the spin-reorientation field B_{SF} . Inset: ESR spectra with magnetic fields $B||c$ at $f = 266$ GHz. Dashed lines mark the resonance position at $T = 2$ K. Arrows indicate resonances.

weakly correlated anisotropic magnetic moments in LiFePO_4 . Comparing the nonlinear contribution M_{qf} with a simple Brillouin function (see Fig. 4) indicates a more complex behavior of the extra moment as compared to completely isolated spins $S = 2$. This is particularly evident when the derivative $\partial M/\partial B$ is considered which—in addition to general right bending of M_{qf} —shows two anomalies at $B_1^* = 1.1$ T and $B_2^* = 1.8$ T.

B. High-frequency electron spin resonance

While HF-ESR is susceptible to collective magnetic excitations, at $q = 0$, observation of magnon modes in LiFePO_4 is challenging due to large single-ion anisotropy and strong exchange interactions which lead to large excitation gaps at zero magnetic field of 1446 and 2072 GHz [15,18,19]. When external magnetic fields are applied along the magnetic easy b axis, collective resonance modes are however expected to soften in fields similar to the spin-reorientation field B_{SF} [20]. This is indeed observed in the HF-ESR spectra measured for $B||b$. The spectrum obtained at 348 GHz (Fig. 5, blue line) features the two expected resonances close to $B_{\text{SF}} = 32$ T. In addition, two resonances with less intensity at lower fields are observed. Applying magnetic fields $B||c$, i.e., where below the zero-field splitting no magnon modes are expected, yields a spectrum (black line) with at least one clear resonance of low intensity. One has to conclude that the weak features are not associated with magnon modes. Instead, the temperature evolution of the intensities of the weak resonance features implies a Curie-like behavior. This is demonstrated by spectra taken at 266 GHz and for $B||c$ displayed in the inset of Fig. 5. The spectra display rather intense peaks at ~ 0.5 and ~ 4.4 T as well as weaker slightly split resonances at ~ 2.3 T. All these features show Curie-like behavior as the integrated intensities decrease upon heating, thereby resembling the Curie-like

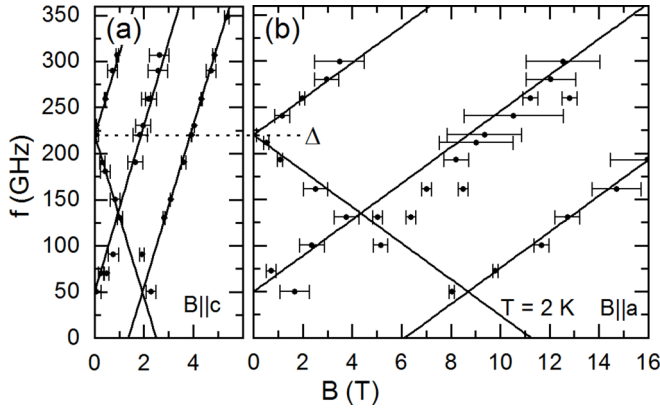


FIG. 6. Frequency dependence of resonance fields at 2 K with external magnetic fields (a) $B||c$ and (b) $B||a$. Solid lines are linear fits to the resonance branches. The dashed line indicates the zero-field splitting Δ .

upturn of magnetic susceptibility [see Fig. 2(a)]. Yet from the energy level diagram Fig. 1 a rather constant intensity of the first feature between 2 and 4 K is expected.

The measured frequency dependencies of the resonance fields displayed in Fig. 6 for magnetic fields $B||c$ and $B||a$, respectively, allows us to clarify the microscopic origin of these resonances. The general behavior of the resonance branches is similar for both magnetic field directions. All resonances are associated with resonance branches with linear field dependence of resonance frequency and, except for the sign, similar slopes for a given field direction. Though small curvature of the resonance modes cannot be excluded. In addition, for each field direction we observe two gapped modes of opposite slope with zero-field splitting of $\Delta = 220(3)$ GHz. At approximately ~ 50 GHz, the falling branches cross or turn into an increasing mode. Such crossing of spin states is typically associated with anomalies in the static magnetization and it indeed nicely accounts for the anomaly B_2^* (see Fig. 4). Figure 1 indicates that this crossing of ground state levels is expected to take place at zero frequency and ~ 2.4 T. On the other hand, low symmetric environment can lead to an anticrossing of the energy levels. The experimental data (see Fig. 6) do not allow us to clearly discriminate between these scenarios. Finally, there is an additional mode with positive slope. Considering the same g factors for all branches yields zero-field splitting of $\Delta' \sim 50$ GHz while allowing for the variation of g results in $\Delta' \sim 20$ GHz. Note, however, uncertainties due to the fact that the linear behavior might not extend to the lowest field so that Δ' may be within these two limiting cases. The observation of three resonance branches indicates that at least a spin $S = 3/2$ model is needed to describe the data. However, the observation of two different zero-field splittings suggest an effective spin $S = 2$ model, because in a $S = 3/2$ system one ungapped resonance line is expected due to Kramers theorem.

The slopes of the branches allow determining the respective effective g values which in the following will be just named g values. As mentioned above, the slopes and hence the g values of all branches of each direction are equal within error bars while there are large differences for the different

field orientations. Quantitatively, the data in Fig. 6 imply $g_c = 6.3(1)$ and $g_a = 1.4(1)$ [23]. The observation of a large g value for $B||c$ and a rather small one for $B||a$ is fully consistent with the anisotropic Curie-like upturn of the susceptibility. The measured anisotropy $(g_a/g_c)^2$ would yield $C_a = 0.009(2)$ erg K/G² mol.

IV. DISCUSSION

Both static and dynamic magnetic studies evidence the presence of anisotropic magnetic moments which are not involved in long-range antiferromagnetic order. As Fe moments in the ground state are slightly tilted, it is illustrative to compare the resonance branches presented above with modes originating from tilted moments which, e.g., are observed in α -Fe₂O₃ [24], α -Cu₂V₂O₇ [25], and Sr₂IrO₄ [26]. In all examples, low-energy excitation modes show bending, i.e., are clearly nonlinear and exhibit stronger anisotropy of the effective g values as observed in LiFePO₄. In addition, the resonance modes of tilted moments are usually not observed for all magnetic field directions. This further confirms that extra moments in LiFePO₄ are not associated with the long-range ordered ground state of Fe²⁺ moments on Fe lattice sites. Instead, defects which are strongly associated with the crystallographic lattice of LiFePO₄ are accountable for the observed anisotropic Curie-like response. We note that this conclusion is supported by the fact that the saturation value $M_{\text{qf}}^{\text{sat}}(B||c)$ of the quasifree component of the magnetization is sample dependent.

The obtained Curie-constant C_c , the saturation magnetization of the extra moments $M_{\text{qf}}^{\text{sat}}$, and the g -value g_c enable determining the effective total angular momentum quantum number

$$J = \frac{C_c}{M_{\text{qf}}^{\text{sat}}} \frac{3k_B}{\mu_B N_a g_c} - 1 \quad (1)$$

of the impurities, with N_a the Avogadro constant. This procedure yields $J = 2.16(9)$ which is close to the integer $J_{\text{eff}} = 2$ and hence suggests attributing the anisotropic moments to Fe²⁺ impurities with high spin $S = 2$ and quenched orbital momentum $L \approx 0$. This leads to a density of impurities of $n = 0.0053(7)$ /f.u. The phenomenological description of the susceptibility by means of a Curie-Weiss-like law is a sufficient approximation. Using a more sophisticated analysis and including the energy level splittings directly in the analysis results in an impurity density of $n = 0.0057$ /f.u., see the Supplemental Material S3 [27].

Low-temperature increase of the susceptibility is not only observed for LiFePO₄ but was reported previously for other phosphates, too. In LiMnPO₄ it however shows isotropic Curie-like behavior [10]. This discrepancy is attributed to an isotropic g factor expected for half-filled d shell of Mn²⁺ ions. For LiMn_{1-x}Fe_xPO₄ it was observed that with increasing iron content the Curie-like susceptibility upturn is getting more anisotropic [10]. An even stronger increase of the susceptibility in c direction is reported for LiFePO₄ doped with nonmagnetic Mg ions [28]. Our results suggest that this behavior is directly linked to the increase of antisite disorder.

The crystal structure exhibits four different Li sites with the same local distorted octahedral oxygen environment. The

distorted octahedra exhibit C_1 symmetry and are positioned in the crystal structure in a way that always the same facet of the octahedron is normal to the c axis of the crystal structure. The octahedra are however rotated in the ab plane. For Fe at a Li position, the low-symmetry coordination hence fully lifts orbital degeneracy which results in orbital splitting into separated $m_s = \pm 1$ and $m_s = \pm 2$ doublets and a singlet $m_s = 0$. This general energy level schema is confirmed by the HF-ESR data as the observed low-field ESR branches are straightforwardly associated with allowed transitions between split spin states of localized $S = 2$ (see Fig. 1). In particular, the modes with zero-field gap of $\Delta = 220(3)$ GHz display transitions between $m_s = \pm 1$ and $m_s = \pm 2$ states and Δ quantifies their splitting in zero field. While the resonance branch with $\Delta' \sim 50$ GHz is associated with transitions between $m_s = 0$ and $m_s = \pm 1$ states. Consequently, anomalies B_1^* and B_2^* in the magnetization curve signal the changes of the magnetic ground state from $m_s = 0$ to $m_s = -1$ and $m_s = -1$ to $m_s = -2$, respectively. The phenomenological model used accounts for the main features found in the magnetization both at low and high magnetic fields and at different temperature as well as for the field dependence of the EPR resonances. The observed effective g value of $g = 6.5$ indicates that orbital contributions are not a small perturbation. Due to the unknown relaxed atomic structure in the vicinity of the defects, no detailed modeling of the single-ion anisotropy was done.

Comparing our experimental results to materials with paramagnetic Fe^{2+} ions in a low-symmetry coordination, the here observed zero-field splitting of the energy levels is in the common range [29,30]. In contrast, the effective g value, respectively the g -value anisotropy observed in our study, is unusually high as, e.g., in $\text{Mg}_2\text{SiO}_4:\text{Fe}$ where Fe^{2+} ions are on octahedral sites of the forsterite structure, anisotropic g values of $g_{\parallel} = 4.30$ and $g_{\perp} = 2.0$ are observed [31].

Since formation of defects depends on details of the synthesis process, Fe^{2+} -antisite density is supposed to vary between different samples and different parts of the crystalline rod obtained by our optical floating-zone method. Indeed, while $n = 0.53(7)\%$ is obtained from the analysis of magnetic data above, a different part of the same single crystalline batch which exhibits identical T_N shows $n = 0.32\%$ (see the Supplemental Material [27]). Both values are in perfect accordance with the expected equilibrium defect concentration of 0.1% to 0.5% for the used solid-state synthesis temperatures [3].

In comparison with other experimental methods, our results quantitatively agree to determination of antisite disorder by lithium diffusion experiments on crystalline nanoplatelets of LiFePO_4 , where 0.5% antisite concentration was obtained [5]. Diffraction studies illustrate the large regime of potential antisite defect concentrations in LiFePO_4 . High concentrations can be, e.g., due to insufficient solid state diffusion so that values of 7% to 8% have been reported for materials from hydrothermal and high-temperature solid state synthesis methods [32]. The growth method of single crystals implies rather diverse antisite concentrations as flux-grown LiFePO_4 is reported to exhibit no evidence for antisite defects in these samples [33] from a combination of powder and single crystal diffraction (x ray and neutron). While synchrotron powder x-ray diffraction data on ground crystals grown by the optical floating-zone (TSFZ) method at ambient pressure imply

values of 2.5% [34]. Laboratory powder XRD data on single crystals of the same batch as studied here have been refined when antisite concentration of $n = 0.023(2)/\text{f.u.}$ [10] was considered, which is larger than the concentration of quasifree $S = 2$. We attribute this to the uncertainty of the powder XRD method with respect to a particular kind of defects [33]. We conclude that in addition to the particular paramagnetic-like type of defects associated with Fe^{2+} on Li sites, further defects types may be included in the values provided by Rietveld analysis of conventional x-ray patterns. We emphasize, in this respect, that our magnetic studies can discriminate between different defects. While nonmagnetic ones are not detected, different magnetic defects would result in different g factors and zero-field splittings which is not observed. We mention that failure of detecting Li-Fe antisite defects by means of X-band ESR in Ref. [35] is fully inline with the fact that zero-field splitting is larger than 10 GHz (see Fig. 6) which prevents detection in conventional X-band ESR.

In addition, our results imply that in theoretical studies on electronic properties and antisite-defect mediated diffusion in LiFePO_4 , orbital degrees of freedom should be taken into account, which can be concluded from the highly anisotropic g factor of the defect moments. In particular, a local structure model as used in Ref. [6] cannot account for these features. In general, DFT calculations of antisite defects [9] should yield the anisotropic g values as well as zero-field splitting due to crystal field effects which may be used to confirm the validity of a numerical approach.

Knowledge of the strongly anisotropic g values also enables us to quantitatively determine antisite disorder by static magnetometry even in LiFePO_4 powders. A Curie-Weiss fit to the volume magnetic susceptibility in the temperature region of 2 to 20 K results in a powder averaged Curie constant C from which the defect concentration

$$n = \frac{3C k_B}{2\mu_B^2 N_A (g_a^2 + g_b^2 + g_c^2)} \quad (2)$$

is obtained by using $g_a = 1.4$, $g_b = 2.0$, and $g_c = 6.3$.

V. SUMMARY

Our detailed studies of the static and dynamic magnetic properties on single crystals by means of magnetization and high-frequency electron spin resonance measurements enable qualitative and quantitative conclusions on the nature and the properties of antisite defects in LiFePO_4 . The presence of rather localised moments, which are only weakly magnetically interacting with the magnetic subsystem on the crystallographic Fe positions, is attributed with Fe^{2+} ions on Li positions. The fingerprint of these moments includes linear resonance branches, a highly anisotropic g factor with $g_a = 1.4$, $g_b = 2.0$, and $g_c = 6.3$, and significant zero-field splittings of $\Delta = 220(3)$ GHz and $\Delta' \sim 50$ GHz. We demonstrate a procedure to precisely determine the defect concentration by static magnetization measurements on powder materials.

ACKNOWLEDGMENTS

The project is supported by Deutsche Forschungsgemeinschaft (DFG) through KL 1824/13-1 and by Bundesministerium für Bildung und Forschung (BMBF) via the SpinFun

project (13XP5088). We acknowledge the support of the HLD at HZDR, member of the European Magnetic Field Laboratory (EMFL). S.Z. and A.P. acknowledge the support of DFG through ZV 6/2-2.

-
- [1] G. R. Gardiner and M. S. Islam, *Chem. Mater.* **22**, 1242 (2010).
- [2] C. Wang and J. Hong, *Electrochem. Solid State Lett.* **10**, A65 (2007).
- [3] R. Malik, D. Burch, M. Bazant, and G. Ceder, *Nano Lett.* **10**, 4123 (2010).
- [4] J. Yang and J. S. Tse, *J. Phys. Chem. A* **115**, 13045 (2011).
- [5] H. Liu, M.-J. Choe, R. A. Enrique, B. Orvañanos, L. Zhou, T. Liu, K. Thornton, and C. P. Grey, *J. Phys. Chem. C* **121**, 12025 (2017).
- [6] S. Adams, *J. Solid State Electrochem.* **14**, 1787 (2010).
- [7] R. Amin, C. Lin, and J. Maier, *Phys. Chem. Chem. Phys.* **10**, 3524 (2008).
- [8] C. Neef, A. Reiser, E. Thauer, and R. Klingeler, *Solid State Ionics* **346**, 115197 (2020).
- [9] G. K. P. Dathar, D. Sheppard, K. J. Stevenson, and G. Henkelman, *Chem. Mater.* **23**, 4032 (2011).
- [10] C. Neef, H. Wadepohl, H.-P. Meyer, and R. Klingeler, *J. Cryst. Growth* **462**, 50 (2017).
- [11] P. Comba, M. Großhauser, R. Klingeler, C. Koo, Y. Lan, D. Müller, J. Park, A. Powell, M. J. Riley, and H. Wadepohl, *Inorg. Chem.* **54**, 11247 (2015).
- [12] K. Momma and F. Izumi, *J. Appl. Cryst.* **44**, 1272 (2011).
- [13] R. Santoro and R. Newnham, *Acta Cryst.* **22**, 344 (1967).
- [14] J. Werner, S. Sauerland, C. Koo, C. Neef, A. Pollithy, Y. Skourski, and R. Klingeler, *Phys. Rev. B* **99**, 214432 (2019).
- [15] J. Li, V. O. Garlea, J. L. Zarestky, and D. Vaknin, *Phys. Rev. B* **73**, 024410 (2006).
- [16] L. Zhi, D. Nai-Li, K. Zhi-Qi, C. Zhao-Hua, L. Li-Jun, C. Li-Quan, and H. Xue-Jie, *Chin. Phys.* **13**, 2158 (2004).
- [17] G. Rousse, J. Rodriguez-Carvajal, S. Patoux, and C. Masquelier, *Chem. Mater.* **15**, 4082 (2003).
- [18] R. Toft-Petersen, M. Reehuis, T. B. S. Jensen, N. H. Andersen, J. Li, M. D. Le, M. Laver, C. Niedermayer, B. Klemke, K. Lefmann, and D. Vaknin, *Phys. Rev. B* **92**, 024404 (2015).
- [19] Y. Yiu, M. D. Le, R. Toft-Petersen, G. Ehlers, R. J. McQueeney, and D. Vaknin, *Phys. Rev. B* **95**, 104409 (2017).
- [20] T. Nagamiya, K. Yosida, and R. Kubo, *Adv. Phys.* **4**, 1 (1955).
- [21] C. Baumann, G. Allodi, A. Amato, B. Büchner, D. Cattani, R. De Renzi, R. Klingeler, P. Reutler, and A. Revcolevschi, *Phys. B: Condens. Matter* **374**, 83 (2006).
- [22] R. Klingeler, B. Büchner, S.-W. Cheong, and M. Hücker, *Phys. Rev. B* **72**, 104424 (2005).
- [23] Applying magnetic fields along the b axis results in a more complex frequency dependence of the resonance fields with a g value of the main resonance lines of $g_b = 2.0(1)$.
- [24] P. Pincus, *Phys. Rev. Lett.* **5**, 13 (1960).
- [25] L. Wang, J. Werner, A. Ottmann, R. Weis, M. Abdel-Hafiez, J. Sannigrahi, S. Majumdar, C. Koo, and R. Klingeler, *New J. Phys.* **20**, 063045 (2018).
- [26] S. Bahr, A. Alfonsov, G. Jackeli, G. Khaliullin, A. Matsumoto, T. Takayama, H. Takagi, B. Büchner, and V. Kataev, *Phys. Rev. B* **89**, 180401(R) (2014).
- [27] See Supplemental Material at <http://link.aps.org/supplemental/10.1103/PhysRevMaterials.4.115403> for a quantitative analysis of the low temperature magnetic susceptibility.
- [28] D. Chen, X. Wang, Y. Hu, C. Lin, S. Dou, and R. Nigam, *J. Appl. Phys.* **101**, 09N512 (2007).
- [29] J. Krzystek, A. Ozarowski, and J. Telsner, *Coord. Chem. Rev.* **250**, 2308 (2006).
- [30] C. Rudowicz and H. Wai-fong Sung, *J. Phys. Soc. Jpn.* **72**, 61 (2003).
- [31] G. Shakurov, T. Shcherbakova, and V. Shustov, *Appl. Magn. Reson.* **40**, 135 (2011).
- [32] S. Yang, Y. Song, P. Y. Zavalij, and M. S. Whittingham, *Electrochem. Commun.* **4**, 239 (2002).
- [33] Y. Janssen, D. Santhanagopalan, D. Qian, M. Chi, X. Wang, C. Hoffmann, Y. S. Meng, and P. G. Khalifah, *Chem. Mater.* **25**, 4574 (2013).
- [34] R. Amin, J. Maier, P. Balaya, D. Chen, and C. Lin, *Solid State Ionics* **179**, 1683 (2008).
- [35] R. Amin, P. Balaya, and J. Maier, *Electrochem. Solid State Lett.* **10**, A13 (2006).